Jet probes of quark-gluon plasma: experiment and simulation

Eleanor Gentry

Thesis Advisor: Jamie Nagle, Department of Physics
Honors Council Representative: John Cumalat, Department of Physics
Outside Reader: Magdalena Czubak, Department of Mathematics
Additional Committee Member: Dennis Perepelitsa, Department of Physics

A thesis presented for the degree of
Bachelor of Arts

Department of Physics
University of Colorado Boulder
Boulder, Colorado, USA
April 9, 2024

Abstract

When heavy nuclei hit each other at almost the speed of light, a new state of matter termed "quark-gluon plasma" (QGP) is briefly produced. In these collisions, the particles with the highest momenta that later form "jets" move through the plasma and lose some of that momentum because of the very strong interactions. It is impossible to directly observe the QGP because it is too short lived, but it is possible to measure the energy of the jets produced and compare them to jets from collisions that do not have a QGP. The comparisons can help quantify the extent to which the jets have lost energy. This, combined with other information about the collision, can help characterize the expansion and flow of the plasma. These collisions are being studied experimentally in the sPHENIX detector and can also be simulated. In this thesis, we explore the experimental methods used at the sPHENIX detector, as well as the construction process for new detectors. Additionally, we present preliminary results from a publicly available Monte Carlo simulation called Jewel. The results suggest that "jet quenching" is occurring, which means that Jewel is likely a valuable tool to explore low momentum jet kinematics.

Acknowledgements

This thesis would not have been possible without the incredible mentorship and guidance of Professor Jamie Nagle. He has inspired me to become a better scientist and researcher. I am also very grateful for Professor Dennis Perepelitsa, who was always willing to help me understand the most complex topics and offered mentorship and advice whenever I needed it. The members of my lab group were also instrumental in my success, offering me resources, knowledge, code snippets, wisdom, and compassion. Without these people, I would not have been able to successfully learn so much about this wonderful field.

Dedication

This thesis is dedicated to those in my life who have encouraged me to engage with my passions. I want to thank my family, my mom, dad and two cats for loving me and giving me every opportunity to grow and change with every budding interest. I also want to thank my found family, Nick, Sophie, Morgan and Julia, who taught me that a community is more than just the group of people around you. In particular, I want to thank my partner, Nick, because I can't think of a better person to grow into a physicist with. I want to thank all of the physics professors who humored my questions, discusses far out topics with me, and cared enough to teach me physics but also how to think like a physicist. Additionally, I am very grateful for the women and gender studies department; without their support and refuge, I would have struggled to believe in myself as a woman in science. I also would not have been able to graduate without the support of the physicians and nurses who helped me navigate difficult life challenges in a way that gave me the freedom to study and learn as much as I wanted to. In particular, I want to thank the nurses at the infusion center for encouraging me, making sure I'm taken care, and listening to me ramble about physics with enthusiasm and kindness. And finally, this thesis is dedicated to my sister, Charlotte. She is my person, and she makes me better every day.

Contents

1 Introduction

The Standard Model offers crucial insight into what happens inside of an atom. The matter that makes up the nucleus of atoms is dominated by the strong nuclear force. At length scales that are less than the size of a nucleon (around 10^{-15} m) the strong nuclear force dominates the particle interactions over the other forces. In order to observe the inside of a nucleon, we must study the interactions and scattering that occurs during high energy collisions.

One way to study the effects of the strong force is with particle collisions. Physicists accelerate particles to almost the speed of light and hit them together. Because these collisions are so energetic, the strong force can no longer hold the subatomic particles together. They break apart and produce enormous amounts of energy along with rare types of particles. Observing the results of these collisions has helped develop the Standard Model by identifying the produced subatomic particles.

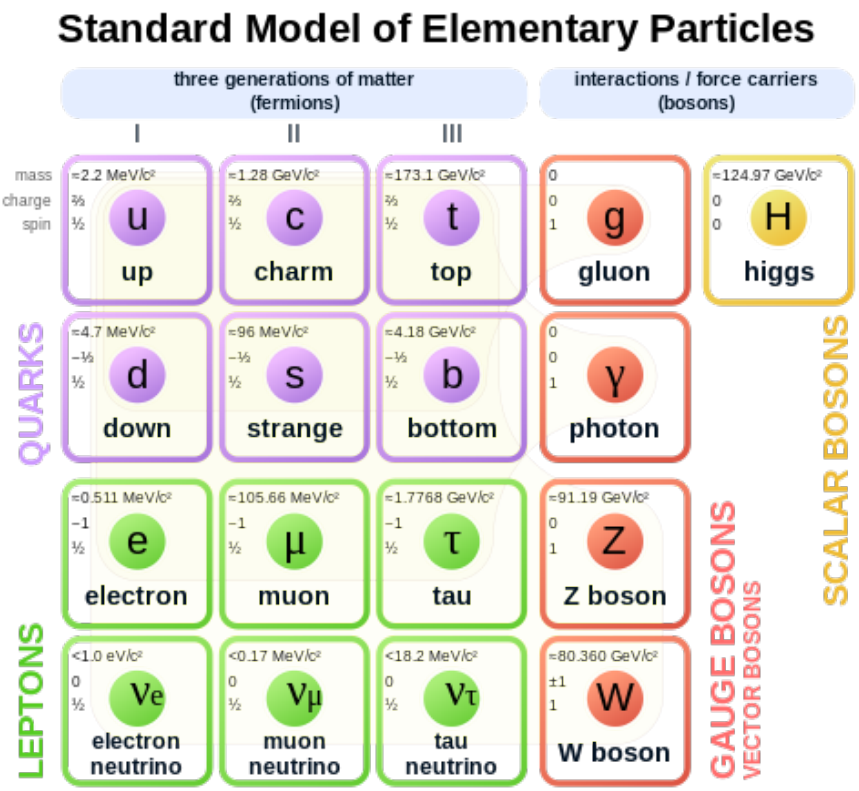

Figure 1: The Standard Model of elementary particles. The purple section shows quarks, the massive partons inside hadrons. The red section shows force carriers including gluons, which are the carriers of the strong nuclear force. The interactions via gluons are governed by Quantum Chromodynamics (QCD). Figure reproduced from Ref. [1].

In particular, colliding two heavy nuclei such as lead or gold will cause deconfinement of the quarks and gluons when the strong force is overcome by the collision energy. Protons and neutrons are primarily comprised of quarks, the top left section of the Standard Model - see Figure 1). Quarks are held together by gluons, which is literally the "glue" of the strong force (top right of Figure 1). Quarks and gluons are point-like particles called partons that make up the hadronic matter of a nucleus like protons and neutrons. If the energy density of the matter is high enough, the collision will produce a state of matter called the quark-gluon plasma (QGP).

The QGP produced in heavy ion collisions only exists for 10^{-23} seconds. This makes it very difficult to observe because the detectors can't be close enough to the collision and the resolution of the detectors is not fast enough. By comparing the highest energy particles produced in heavy ion collisions with the highest energy particles produced in proton-proton collisions, it is possible to observe how interactions with the QGP medium influence the particles emitted from the collision. The interactions of high energy particles with the QGP is referred to as "jet quenching."

The Relativistic Heavy Ion Collider (RHIC) at Brookhaven National Laboratory (BNL) is dedicated to studying the QGP. RHIC has been colliding heavy ions since 2000, and the newest experiment sPHENIX is expected to collect massive amounts of data for the study of the strong force in QGP matter. sPHENIX took its first data in the summer of 2023 after multiple years of detector design, research and development, construction, and installation. Most of the run time in 2023 was used to calibrate and fine-tune the detectors, referred to as commissioning. Predictions from theory will be needed to interpret the forthcoming physics data from sPHENIX.

Heavy ion collisions can also be studied with simulations based on analytical models of the QGP. JEWEL is a publicly-available simulation program that uses a Monte Carlo technique to predict the location of partons after a collision given their initial positions [2]. This computer program was developed for and is primarily used to model heavy ion collisions at high energy for the Large Hadron Collider (LHC). The collisions at RHIC are an order-of-magnitude lower energy than the collisions at the LHC. This means the QGP doesn't exist for as long, which makes it easier to study the phase transition from hadronic matter but also harder to observe the jet quenching within the QGP. Both energies have important physics goals and are optimized for studying different kinds of physical phenomena. Lower momentum collisions tend to have more information about the structure and details of the jets. JEWEL was designed with LHC energies in mind, and has not been used extensively for the lower energy collisions that RHIC produces. Because the two colliders operate in such different energy regimes, it is worth investigating the use of JEWEL at lower energy ranges further.

In this thesis, we examine JEWEL's effectiveness at simulating the collisions expected to be observed at sPHENIX, as well as the construction and process of experimentally examining the quark-gluon plasma. First, we will describe the theory behind the quark-gluon plasma, including the motivation to study its properties (Section 2.1). Then, we will discuss the experimental methods used to create and observe the QGP (Section 2.2). We will also discuss the theory behind the computational methods applied in this research (Section 2.3). Then, we will outline the specific contributions made to sPHENIX's Event Plane Detector, specifically construction and testing of the detector tiles and the readout electronics (Section 3). Finally, the results of the simulation will be presented, as well as relevant results from the analysis of that simulation (Section 4).

2 Background Information

2.1 Theory

The strong nuclear force is governed by the field theory Quantum Chromodynamics (QCD). QCD is a non-abelian gauge theory, so the particles governed by QCD are not commutative. The two dominant formulations of QCD used to analyze quark gluon plasma are lattice QCD (lQCD) and perturbative QCD (pQCD). Both theories are only applicable in certain energy and length regimes,. but are nonetheless crucial to understanding and predicting the results of heavy ion collisions. Lattice QCD assumes that quarks are positioned on a lattice and gluons fill in the space between the quarks. Predictions from lQCD have found the mass of the proton with less than 2 percent error ([3]), as well as the transition between hadronic matter and QGP matter occurring at an energy of 156 MeV [4], which is similar to experimental values. Perturbative QCD assumes that the coupling between color charged particles is very small at small distances or high energy, so perturbative techniques can be used.

The QGP is the most perfect known fluid in the universe. This means that the ratio of the shear viscosity

to the entropy is closer to $1/4\pi$ than other material researchers know of:

$$\frac{\eta}{s} \geq \frac{1}{4\pi} \tag{1}$$

[5]. The gradient in velocity perpendicular to the direction of flow within a fluid causes a force that is also perpendicular to the direction of flow. That force is called the shear viscosity. The particles change direction and either slow down or speed up to match the particles nearby, ultimately leading to an equilibration of the flow. Most fluids that are close to perfect, like superfluids, have an extremely low shear viscosity. The particles have almost no interaction, so they flow past each other and don't apply a very big force on each other. However, the QGP fluid is strongly coupled, meaning that the forces between particles are strong, which does not allow for an extremely low shear viscosity. Instead, it's the incredibly high entropy density that makes the QGP a nearly perfect fluid. Because the collisions occur at such a high energy, the entropy of the system is enormous, which ultimately means that despite the fact that η is not very small, $\frac{\eta}{s}$ is, bringing the overall value closer to $\frac{1}{4\pi}$.

As baryonic matter becomes more dense or as the temperature increases, hadrons will reach a first order phase transition and the gluons will not hold the quarks together anymore.

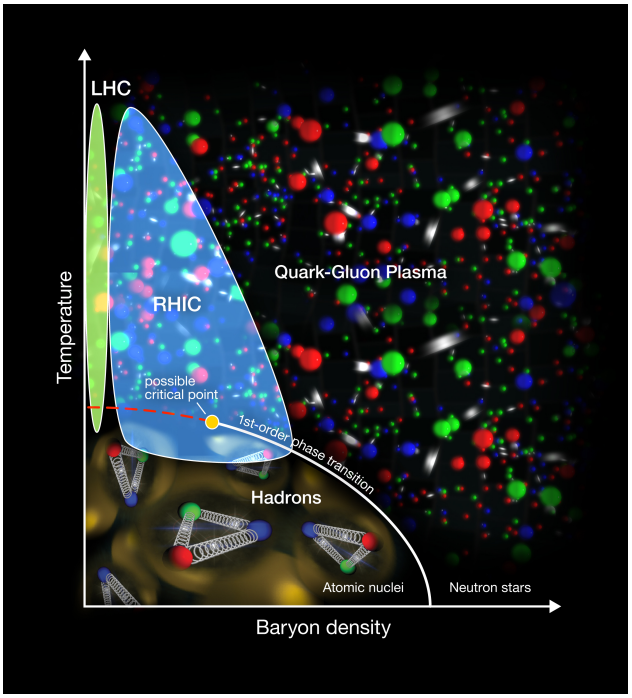

Figure 2: The phase diagram of the quark-gluon plasma. The x-axis of the figure is the baryonic density, and the y-axis is the temperature. Particle colliders like the Large Hadron Collider and the Relativistic Heavy Ion Collider cause the colliding particles to reach temperatures high enough to cross into the QGP regime, overcoming the strong nuclear force. Figure reproduced from Ref. [6].

The QGP can be described as its own state of matter, and a phase diagram can be a useful way to understand the conditions required to create the QGP, as shown in Figure 2. When the density of baryonic matter gets very high or when the temperature gets very high, the hadrons present will overcome the strong nuclear force and their partons (quarks and gluons) will flow freely. This first order phase transition has been modeled or observed at most baryon densities and temperatures. At low density but high temperatures there is a theorized critical point. At lower temperatures or lower baryonic density, hadronic matter exists. Figure 2 shows the regime where hadronic matter is stable below the first order phase transition.

The phase transition between hadronic matter and QGP is theorized to be first order due to results from

lattice quantum chromodynamics. The phase transition is due to asymptotic freedom and gauge symmetries [7]. At low temperatures and low baryonic densities, the matter inside of nucleons is dominated by the strong nuclear force over any other kind of force. Because the strong nuclear force attracts particles of different color charges, the positively charged protons are held together despite electromagnetic repulsion. However, the strong nuclear force decreases with distance, so it is only able to dominate over the electromagnetic force on length scales less than 10^{-15} m, which is approximately the diameter of a nucleus [7].

When quarks are pulled apart, the strong nuclear force between them decreases at first, but then starts to increase. The quarks will either be pulled back together or a quark-antiquark pair will spontaneously appear from the potential energy between the quarks, mediated by the strong force. The potential between the quarks is defined as

$$V(r) = -\frac{A(r)}{r} + K_r, \tag{2}$$

where $A(r)$ is a function that describes the coupling or interaction between the quarks, and K_r is a linear confinement term [8]. This equation is only valid on short length scales. Outside of the size of a nucleon, it becomes energetically unfavorable for the two quarks to be confined to each other, which causes spontaneous quark-antiquark particle production. The potential energy from Equation 2 is converted into the mass of the new particles via Einstein's famous equation, $E = mc^2$. The new particles will each be bound to one of the original quarks [4].

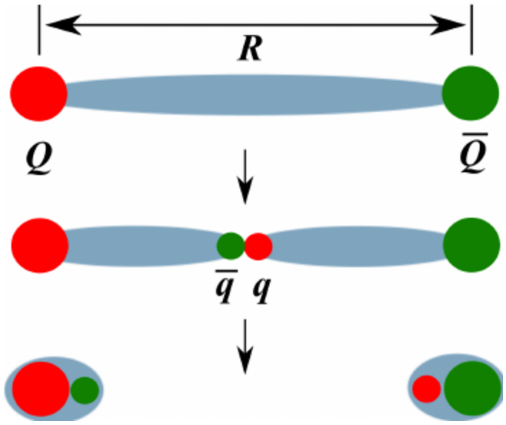

Figure 3: This image shows the process of spontaneous particle production as a result of asymptotic freedom. The strong nuclear force increases as the distance between particles increases, so as two quarks confined by a gluon are pulled apart, the force between them gets very large. Eventually a quark-anti-quark pair will be spontaneously generated from the energy between the original quarks, forming two new bonded sets of quarks. Figure reproduced from Ref. [9].

Figure 3 shows this process occurring for a meson, where the quarks are pulled away from each other and the gluon is stretched. The force between the quarks increases with distance and when the force becomes large enough, a quark-antiquark pair is produced and they are each bound to one of the original quarks with a gluon between them. This concept won the Nobel Prize in 2004 and is now foundational to understanding the strong nuclear force.

The Big Bang had extremely high temperatures and extremely high baryon density, so for the first 6 microseconds, the entire universe was a quark gluon plasma. The expansion of the early universe can be recreated in the lab by colliding heavy nuclei together at high speeds (colloquially referred to as a "Little Bang"). Although the baryonic energy density of these collisions is relatively low, the temperature is on the order of 10^{12} K, above the theoretical transition energy of 156 MeV [4], so a quark-gluon plasma can be produced. Before big bang nucleosynthesis (BBN), the universe was almost entirely a quark-gluon plasma because it was extremely dense and had an extremely high temperature.

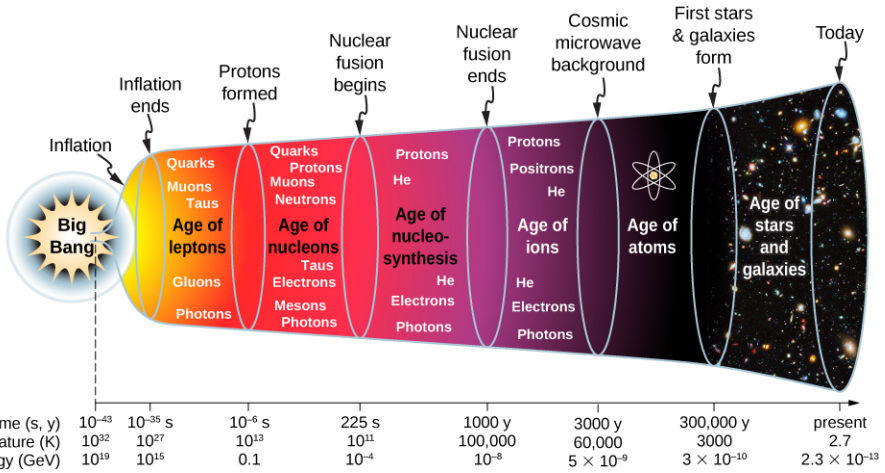

Figure 4: The evolution of the universe after the big bang. In the "Age of Leptons" before 10^{-6} seconds, the quarks and gluons flowed freely around each other. Once the universe had expanded enough and cooled down enough, the strong nuclear force overcame the kinetic energy of the partons and organized matter into hadronic matter like protons and neutrons. Figure reproduced from Ref. [10].

The quark gluon plasma created in colliders like the LHC and RHIC modes the evolution of the early universe. The "little bangs" begin with high energies above the around 150 MeV threshold to create a QGP. After the collision, the particles expand outwards at relativistic speeds, causing them to cool and eventually "freeze-out" back into hadrons. This occurred after the big bang when the universe cooled below 150 MeV and the strong nuclear force organized the partons into hadrons.

2.2 Experiment

Most collisions produce a few groups of highly energetic particles, usually two in about opposite directions because of momentum conservation. These groups of particles are called jets. Jets are one of the most effective ways to characterize the QGP because the jet energy is influenced by its interaction with the QGP medium, usually losing energy as it traverses the fluid. This phenomenon is called jet quenching. Figure 5 shows how the jet might traverse the QGP. Two quarks hit each other, or experience hard scattering. As the partons produced bounce off each other and go in opposite directions, they might experience radiative energy loss, or soft scattering, represented by the curly lines within the orange QGP matter. Once the particles exit the QGP, two highly energetic particles are left to observe, represented by the green arrows [11].

It is impossible to observe the QGP directly because it freezes out before it could possibly reach any of the detectors. Therefore, experimentalists rely on the jets to learn about how the quark-gluon plasma behaves. The jet energy observed is compared to the jet energy in collisions that don't produce quark-gluon plasma, like proton-proton collisions. The proton-proton collision energies are scaled up by mass to be the same as the nuclei and the produced jets are compared. Although there are many ways to characterize jet quenching, the most useful here is the nuclear modification factor, or

$$R_{AA} = \frac{\frac{1}{N_{evt}} \frac{d^2 N_{jet}}{dp_T dy}}{< T_{AA} > \frac{d^2 \sigma_{jet}}{dp_T dy}}, \tag{3}$$

which is the change in jet momentum ($\frac{d^2 N_{jet}}{dp_T dy}$) scaled by the number of events ($\frac{1}{N_{evt}}$) divided by the nuclear thickness function ($< T_{AA} >$) times the cross section of proton-proton collisions ($\frac{d^2 \sigma_{jet}}{dp_T dy}$) [13]. The higher the R_{AA}, the more the jets are quenched.

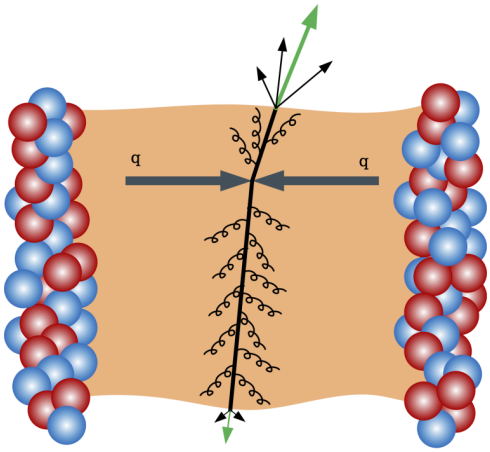

Figure 5: This schematic shows how the QGP forms from the two incoming nuclei on either side of the image. The QGP medium between them causes deconfinement of the partons from their protons and neutrons. When two of the partons hit each other directly in hard scattering, like the two quarks represented by the horizontal arrows, they bounce off each other and move through the QGP. The curly lines represent the fragmentation of the partons as they move outwards from the collision. Once the parton exits the QGP it continues to fragment. The original parton or its subsequent particles, along with nearby particles that were dragged along with the high energy parton are then able to be identified as a jet. Figure reproduced from Ref. [12].

The accelerators that produce the QGP through heavy ion collisions need very specialized equipment to actually observe the results of those collisions. The sPHENIX detector is an upgrade of the PHENIX (Pioneering High Energy Nuclear Interaction eXperiment) at RHIC.

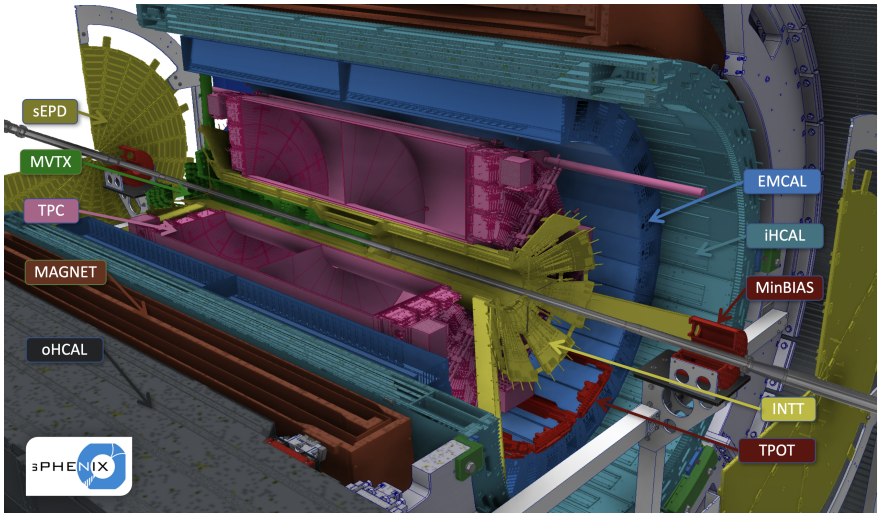

Figure 6: sPHENIX's detectors. Each detector collects a different kind of data or tells the detectors to begin collecting data. CU Boulder participated in the development and construction of the sEPD, or sPHENIX Event Plane Detector. Figure reproduced from Ref. [14].

sPHENIX uses a 1.4 T magnet along with electromagnetic and hadronic calorimeters to detect the energies of particles produced in gold-gold collisions [15]. sPHENIX has newer and better materials than PHENIX, as well as a total azimuthal acceptance for charged particles, and a higher rapidity range. It is important to predict the sPHENIX results because of these differences; PHENIX is different enough that the results are not going to be completely analogous.

The gold nuclei go through many stages before actually being detected by sPHENIX. First, the particles are partially stripped of their electrons and initially accelerated by the booster synchrotron. Then the particles enter the Alternating Gradient Synchrotron (AGS) and are further accelerated. Once the particles have been accelerated to 99.7% of the speed of light and all of the electrons have been stripped away, the particles can be injected into one of the two beams in the RHIC ring, going in opposite directions [16]. They continue to accelerate here, and can stay at near light speeds for several hours while the detectors are taking data.

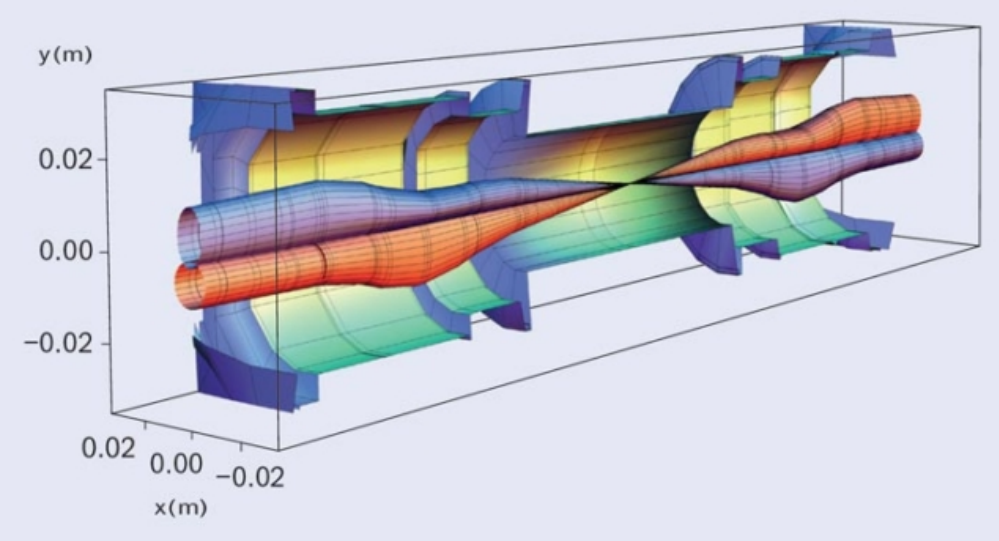

Figure 7: This image shows how the beams at CERN come together within a detector, similar to how the beams at RHIC would come together to interact. The orange and blue beam paths carry particles that move in opposite directions, and the paths of the particles intersect. This small cross sectional area where the particles could come together and actually hit each other is called the interaction region. Figure reproduced from Ref. [17].

Once in the RHIC rings, the gold ions are grouped together in patterns that will collide in the interaction regions at one off the six collision sites, positioned around the ring. sPHENIX is at one of those collision sites. Similar to the mechanism portrayed in Figure 7, the two beams will cross each other, and some of the gold nuclei will get close enough to collide.

Once the particles enter the interaction region, two particles trajectories will completely overlap. Because the particles are moving so quickly, they appear flattened in the lab frame due to special relativistic effects, rather than spherical. Often times, the particles' cross-sectional areas do not completely overlap. The degree of overlap is called the centrality of the collision. When the particles collide, the energy of the partons crosses the threshold of 150 MeV where the particles are no longer confined by the strong nuclear force. A quark-gluon plasma is formed, and the particles flow freely around each other. Despite deconfinement, the particles are still strongly coupled, meaning they are interacting with each other.

Most of the quarks and gluons do not actually hit each other during a collision and interacts via soft scattering, or radiated energy loss. Some particles will hit each other directly, like billiard balls, in a process called hard scattering. The resulting partons from the hard scattering will have the highest momentum out of any parton produced in the collision, meaning that the hard scattered partons will produce the jets. As these partons move away from the site of the collision, the quark-gluon plasma expands and rapidly cools. Once the plasma cools below 150 MeV, the particles will hadronize, or reorganize themselves into bonded quarks and gluons. This occurs in about 10^{-23} seconds, and so the particles are hadronized before they actually hit the detector materials. This process is very similar to the transition from the "age of leptons" to the "age of nucleons" right after the Big Bang, shown in Figure 4.

The collision chamber is surrounded by a huge magnet that produces a 1.4 T field, causing the charged particles to change direction as they move away from the collision. Their curvature depends on their mass and initial momentum, and their energy loss through the detector depends on the individual particle, so by tracking the trajectory of the particles within the magnetic field, it is possible to identify which particle is being detected. This is important because the detectors each only measure one quantity, so the ability to track individual particles over space and time within the magnetic field helps decide which particle is present.

The detectors at sPHENIX have to know when they have to begin taking a data, or when they have to capture a "picture" of a collision. A key component of the trigger system is the Minimum Bias Detector (MBD). This detector is able to identify when incoming particles are likely to collide and tells the other detectors to begin taking data [15]. When a collision occurs, the calorimeters measure the energy of the particles produced in the collision, as the name implies. The electromagnetic calorimeter (EMCal) uses scintillating fibers to detect electrons and photons produced in the collision, and the hadronic calorimeter (HCal) uses steel to interact with the heavier particles, causing light to be emitted again through scintillating material [18].

Four detectors are dedicated to tracking the trajectories of the particles produced in a given collision. The monolithic active pixel sensor vertex detector (MVTX) is very close to the beam pipe and describes the origin of every produced particle. The intermediate silicon tracker (INTT) communicates between the MTVX and the time projection chamber (TPC) to create a continuous track for each particle. The TPC measures the momentum of the particles and relates that to their tracks. The TPC outer tracker (TPOT) is used to adjust the tracking and confirm particle location. This tracking system is able to continuously take data about the location of the particles, and even adjusts for the relativistic effects that come from the particles' extremely high speeds [15].

There is other data that is helpful to know about the collision besides the particles' tracks and momentums. The MBD is able to give a preliminary idea of the centrality of a collision based on the distribution of particles at high rapidity after the collision. The event plane detector (sEPD) is a crucial step in determining the exact location, orientation, and cross section of the collision. Far away from the interaction region, the zero degree calorimeter (ZDC) measures mostly neutral particles and helps to decide which events are worth keeping [15].

After a collision, a series of electronics apply selection criteria to decide which collisions are worth keeping and studying. sPHENIX has a readout rate of 15 kHz, and a collision rate that is often much higher than that, so it is important to make sure that the data that is read out is actually scientifically valuable. Each detector has its own system, but many originally take data into their front-end electronics, the detectors communicate with each other using CERN's Front-End Link eXchange (FELIX). Many systems use machine learning to evaluate how valuable a certain data set is, trained both with their previous collisions and simulations. Then the data is transmitted to the Data Acquisition System (DAQ), where researchers can access it and do analysis [19].

2.3 Computation

A key tool in the field of heavy ion collisions is the comparison of experimental data with computer models of quark gluon plasma formation and evolution. It is then important to validate these computer models and make sure the comparisons with data are actually comparing results that have similar physical significance.

2.3.1 Monte Carlo Simulations

The computer model Jewel (Jet Evolution With Energy Loss) uses the Monte Carlo technique to simulate heavy ion collisions with high-energy jets [2]. It is based on the well tested model for p+p collisions as coded in Pythia-6.3 [20]. Both of these models are publicly available and have well documented code. The Monte Carlo (MC) simulation method uses random numbers to create a large number of random samples in a given

sample space. The random samples are generated with a probability distribution in the space, so they do not necessarily have to be evenly distributed. Then, some computation is performed on each number in the random sample, and the outcome of that computation can describe the expected results of a physical system. For example, numerical integration often involves a Monte Carlo technique where the total sample size is divided by the samples under the line in a given region, and that ratio is compared to the total area of the region to get the area under the curve.

JEWEL's calculation first uses the Glauber model [21] to spacially distribute the partons before the collision. Each quark is then given a momentum using a parton distribution function (PDF) according to the Les Houches Accords PDFs [22]. JEWEL then creates a boost-invariant expansion of a hydrodynamical QGP gas. Each parton is adjusted to a matrix element produced by perturbative QCD [23]. The leading order partons are the jets produced. They can be modified by medium interactions with re-scattering effects, where the jets fragment [23].

One notable aspect of JEWEL is the ability to produce a minimum jet momentum in each collision. While the instance of high momentum jets is low in reality, JEWEL can only use the initial PDFs that will result in jets of a certain momentum. This can cause a bias in the simulation and will artificially change the momentum distribution around that minimum momentum. Additionally, the majority of the events will have momenta close to the given minimum momentum. That makes it difficult to produce enough statistics to analyze at higher momenta. The solution is to run multiple simulations with different minimum momenta and stitch the distributions together.

2.3.2 Jet finding algorithms

FASTJET is a package that identifies jets using the anti-k_T algorithm. The anti-k_T algorithm cycles over every set of particles and calculates the distance between them and weights it to each particle's momentum with the equation

$$d_{ij} = min(p_{ti}^{-2}, p_{tj}^{-2}) \frac{\Delta R_{ij}^2}{R^2}, \tag{4}$$

where i and j represent the particles in question, p_{ti} and p_{tj} are each particle's transverse momentum, R is the given jet radius to look for, and ΔR_{ij} is the unweighted distance between the particles, given by

$$\Delta R_{ij}^2 = (y_i - y_j)^2 + (\phi_i - \phi_j)^2 \tag{5}$$

[24]. FASTJET uses the parton shower JEWEL produces and compares each set of particles [25]. The highest energy group of partons within the given radius are identified as the jets in each collision. Notably, while JEWEL only simulates events above the minimum jet momentum, FASTJET identifies the jets independently, so not all of the identified jets will be above that minimum momentum cutoff. This means that FASTJET will sometimes identify jets well below the minimum momentum cutoff, and will sometimes identify jets that are actually above the chosen radius as two jets. Both of these computational errors need to be carefully considered when analyzing the jets produced. They also compound the statistical bias of the produced distributions in JEWEL, so the correction is necessary to accurately describe the jet momentum distributions produced by a simulation.

3 sPHENIX Hardware Contributions

This project involved opportunities to assist in the construction of the detector sectors for the sEPD. The sectors are made of 1.2 cm thick plastic scintillator with wavelength shifting optical fibers laid in 31 channels throughout the tile [26]. The fibers are held in with optical epoxy, and read out at a connector at the end of the scintillator material. Then the signal travels through long clear optical fibers to be read out by silicon photomultipliers, digitized by analog to digital converter boards, and ultimately collected into the data acquisition system [26].

Figure 8: Two completed scintillator tiles for the sEPD. The epoxy is still drying on the tile to the left, so the weights are holding the WSFs in the channels. The epoxy has dried completely on the tile to the right, so it is possible to see the channels where the fibers have been placed.

In the summer of 2022, construction of the scintillator tiles was taking place at Lehigh University, and we assisted in the process. While at Lehigh, we laid the wavelength shifting fibers (WSFs) in two of the scintillators. The optical epoxy was first laid in the channel that had been created in the scintillator material with a computer numerical control machine. Then, the WSF was placed in the channel, and held in place while additional epoxy was added on top to ensure the fibers would stay in the channel. Then, plastic and weights would be added on top, all while checking to make sure the fibers had stayed in their channels, and the tile would be left to dry until the next day. This process was repeated 31 times for each scintillator sector.

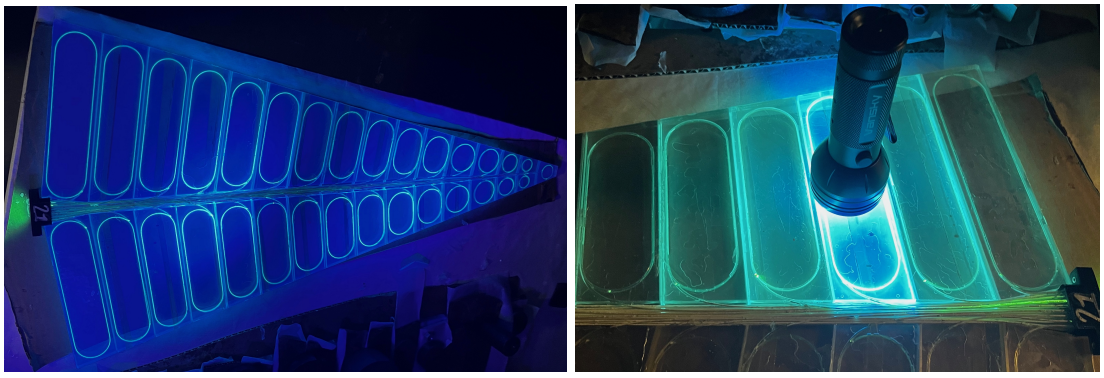

Figure 9: These images show how the scintillator material transports the photons from wherever they are in the tile to the WSFs. The left image shows the process in reverse, where a light is shown into the connector, and the light from the fibers are lighting up each tile. The right image shows how when photons move through the scintillator tile, they are then transported to the WSF. Note that the tiles are very isolated from each other, so one light source is less likely to be detected by multiple tiles.

The WSFs in each tile of the scintillator sectors have a connector at the end of each sector, and then that connector transmits the optical signal to clear fiber bundles to move the data away from the collision

region and to the electronics. We also assisted in the assembly of the clear fiber bundles. First, the optical fiber was unravelled from a large fiber spool. A flashlight was shone down the end of the clear fiber, and the fiber was inspected after cleaning with an alcohol pad while slowly being unravelled. If any light was escaping from the fiber, that section was removed and discarded. Once the fiber was long enough, it was cut and counted to be included in the bundle.

Figure 10: These images show the process of putting the optical fibers through to the connector and polishing them.

Once 31 fibers had been measured, they would be gathered and inserted into plastic tubes to hold the bundle together. Each end was placed into a 3D printed connector and held in place with reflective epoxy. The loose ends of the fibers were cut as closely to the connector as possible without fracturing the structure of the fiber, and then they were sanded down to create a smooth surface. To minimize signal loss, the surface of each fiber was periodically examined with a microscope to ensure no scratches or other obstructions were present. These connectors were then placed against the WSF connectors on the scintillator sectors.

The sPHENIX detectors have over 25,000 channels of calorimeter modules that are read with custom analog to digital converter (ADC) electronics. The sEPD uses these electronics to determine the nuclear collision event plane. The ADC electronics are built at NEVIS Laboratories and then shipped to CU Boulder for testing. Each ADC board was tested along with a transmitter module (XMIT) that control communication between each ADC board.

The signal from the collision is first read out at silicon photomultipliers, then the analog signal is inputted into the ADC board via a pre-amplifier. The ADC boards receive the analog signal, and categorize it into a digital signal based on its shape and amplitude. The digital signal is then read out by the associated XMIT, and then ultimately the data is sent to the data acquisition system.

Each ADC and XMIT board was tested in the summer of 2022 at CU Boulder. First, each board was visually inspected for damage after shipping. Then, a small amount of charge, similar to the charge from a detector module, is injected into the board. The board's response over time is then analyzed, and fit to a known distribution. Each board should respond to the same charge over time so that the data collected by each board is interpreted correctly. If the boards are not responding to the charges predictably, they could skew the data they collect without actually representing the physics of the collision.

If the electronics are responding to the injected charge correctly, then they have to be reprogrammed for token-pass testing. This test ensures that the electronics boards are communicating with the transmitter module correctly. If they are able to communicate correctly, then the boards all pass the testing, and are sent to BNL to be installed.

4 Simulation Results

4.1 Minimum Bias Analysis

After running the simulations in JEWEL and finding the jets with FASTJET, it is important to ensure that the simulation results look reasonable before proceeding with data analysis. One method used to check the realistic extent of simulation results is to plot individual events in space. Figure 11 shows the parton distribution of one event for both proton-proton collisions and gold-gold collisions.

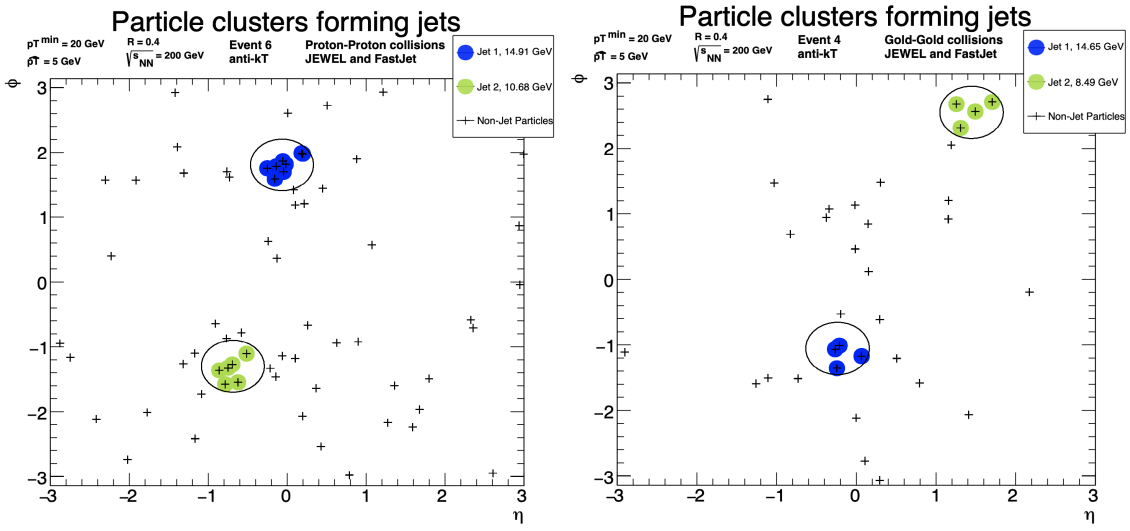

Figure 11: An example collision between two protons (left image) and two gold nuclei (right image) in η - ϕ space. The circles show the FASTJET identified jets, and each jets energy is labeled in the legend. In the left image, no quark-gluon plasma is produced in proton-proton collisions so the jets have not experienced quenching. In the right image, gold-gold collisions produce a quark-gluon plasma, so the jets have lost energy interacting with the QGP medium.

These figures confirm that the simulations produced reasonable results, and the jet finding algorithm is working. There are two clusters of partons in each event that FASTJET identifies as jets. Each jet includes all the nearby particles and does not include far away particles, which says that FASTJET is identifying particles with the correct radius. Each jet is about π apart in ϕ, which means that momentum is conserved. Before the collision, there is no momentum in ϕ, so after the collision, the highest energy particles should go in opposite directions to preserve conservation of momentum.

After visually confirming that the parton showers produced in the simulation appear to be physically realistic, the next step is to identify trends in the jets produced and compare that information between the two simulations. Figure 12 shows the distribution of how many jets are produced at different transverse momenta. These histograms combine six different simulations, each with a different minimum jet momenta, re-weighted to the lowest minimum momentum simulation to create a smooth distribution.

When JEWEL is given a minimum jet momentum, it will artificially inflate the number of jets at that minimum. This computational bias creates an non-physical distribution that does not represent the likely amounts of jets produced at that lowest momentum. This effect is amplified by the jet identification process. FASTJET doesn't know which particles the JEWEL simulation assigned to be a jet, so it might identify jets below JEWEL's cutoff point. However, JEWEL will not produce many events at energies much higher than the cutoff point; the lower energy jets are just more physically probable and that is reflected in JEWEL's calculations. By running simulations with many minimum jet momentums and reweighting the histograms so the distribution is smooth over the whole range of transverse momentums in question, the bias that these computational processes introduce is minimized.

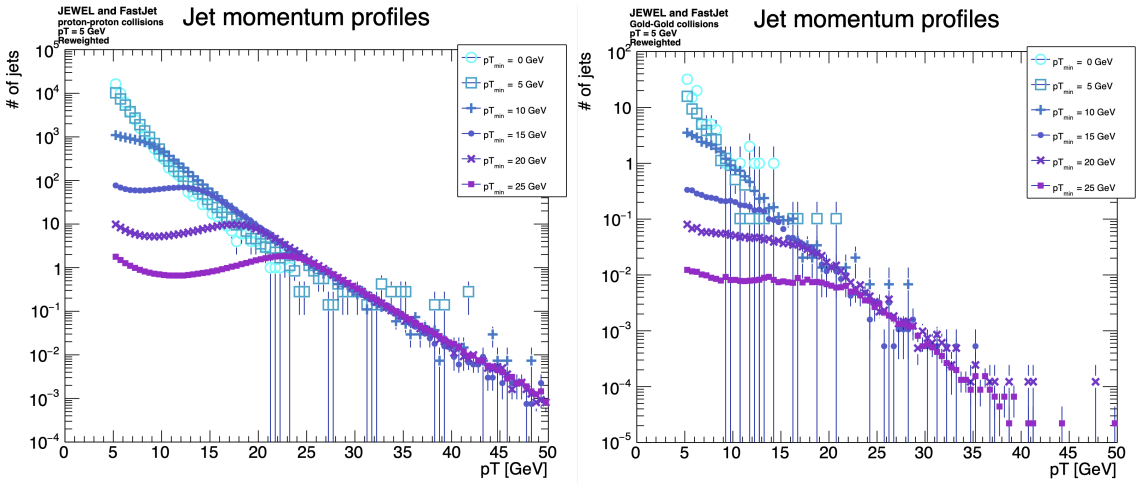

Figure 12: The jet momentum distributions of proton-proton collisions (left) and gold-gold collisions (right). Simulations with many different minimum jet momenta have had their distributions stitched together and re-weighted to the lowest momentum distribution, creating a smooth histogram and minimizing the computational bias.

The histograms in Figure 12 represent the exact same number of events simulated. However, it is clear through visual inspection that while the distributions have about the same shape, the jets resulting from a simulated collision with QGP interaction have a lower momentum. The "quenched" distribution is shifted to the left, meaning that there are fewer jets produced at each momentum than in the unquenched case. If the distributions weren't similarly shaped, this visual inspection would not indicate much about the jet's interaction with the QGP medium. Because the histograms have about the same shape, their different displacement along the p_T axis relative to each other indicates that quenching is occurring in the JEWEL simulations. The next step after confirming that jet quenching is likely is to quantify the extent to which the jets are actually quenched. Two main methods were used to quantify jet quenching in these particular simulations.

4.2 Modified Hagedorn Function

The distribution of the jet momentums for each simulation can describe particle energy loss through QGP interaction when compared to each other. One of the methods to quantify the extent of jet quenching is the modified Hagedorn function,

$$f_2(p_T) = A_2 \frac{p_T^2}{\sqrt{p_T^2 + m_0^2}} (1 + \frac{p_T}{p_2})^{-n_2}, \tag{6}$$

where A_2 is a normalization constant, p_T is the transverse momentum, m_0 is the rest mass of each colliding ion, and p_2 and n_2 are fitting parameters [11]. At each momentum, the fitting parameters were applied to the distribution and the parameters were selected to create a smooth function that was closest to the data. By fitting the two distributions to this function and comparing the coefficients of those fits, it is possible to show jet quenching.

Figure 13 shows the Hagedorn fit for one simulation setup both in the quenched and unquenched case. Because this particular fit is being applied to a simulation setup where bias has not been minimized as described in Section 4.1, the distribution is not as realistic as it could have been with the bias minimization. Therefore the fit was not very good, and differed from the data at some p_T's up to 2.5 times in both cases. In order to improve the quality of the fit, the equation would have to be applied to a momentum distribution that was not influenced by the computational bias introduced by a single simulation. While that particular analysis is definitely possible, there are other ways to quantify the jet quenching that were investigated instead.

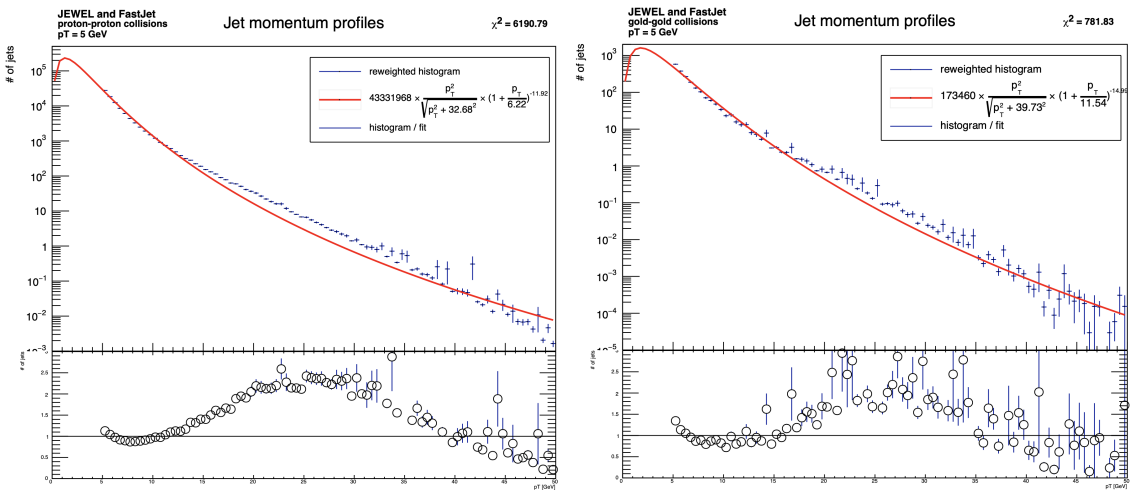

Figure 13: Modified Hagedorn function fit to the momentum distribution of the produced jets. In the left image, the unquenched collisions are simulated. In the right image, the quenched collisions are simulated.

4.3 Nuclear Modification Factor

The best way to quantify jet energy loss as a result of interaction with the quark-gluon plasma is the nuclear modification factor, or the R_{AA}. The nuclear modification factor is defined in Equation 3. This quantity considers how many jets are produced at each momentum for a set number of collisions and compares the jets produced in both quenched and unquenched collisions. The ratio of the number of jets produced in quenched collisions to unquenched collisions as a function of the jet momentum quantifies the extent to which the collisions are quenched over the entire considered momentum range.

When no quenching occurs, the R_{AA} is exactly unity. This means that the jets that interact with the QGP are not losing energy through that interaction. If the jets that move through the QGP were to somehow gain energy, the R_{AA} would be greater than unity. Jet quenching has been proven many times in the field of heavy ion physics [7], so such results are physically impossible. A simulation with an R_{AA} that was 1 or more would indicate a computational process that was not representing physical reality. If the R_{AA} is less than unity, that indicates that the jets are being quenched as predicted. The extent to which they are quenched, or the actual distribution of the R_{AA}, is currently being researched under a variety of conditions.

The results of the simulations presented here show an R_{AA} that does indicate jet quenching. Below a transverse momentum of $p_T = 15$ GeV, the distribution is a result of computational bias, so while the R_{AA} is still within the expected range, it is artificially high between $p_T = 5$ GeV and $p_T = 15$ GeV. Above that minimum jet momentum of $p_T = 15$ GeV, the R_{AA} value is far below 1, as expected. This means that the simulation is quenching the jets when it is asked to consider interactions with the QGP.

It is very promising that the nuclear modification factor appears to be less than 1 in the JEWEL simulations. This means that the parton shower produced by JEWEL is likely considering how particles that move through the QGP will lose energy via interactions with the medium. The R_{AA} value being in the expected regime also indicates that FASTJET seems to be appropriately identifying the jets produced. If the jet locations were not being correctly identified, or if the particles with the highest energies grouped together were not the ones identified as jets, the R_{AA} value might not be below unity where expected.

Further analysis should consider the details of the R_{AA} distribution over p_T, and calculate the R_{AA} value for the bias-reduced distributions described in Section 4.1. Additionally, once sPHENIX has the data available to consider, it will be worth comparing the R_{AA} distribution from JEWEL simulations to the data collected in the experimental collisions observed. While this particular simulation tool has limited use in col-

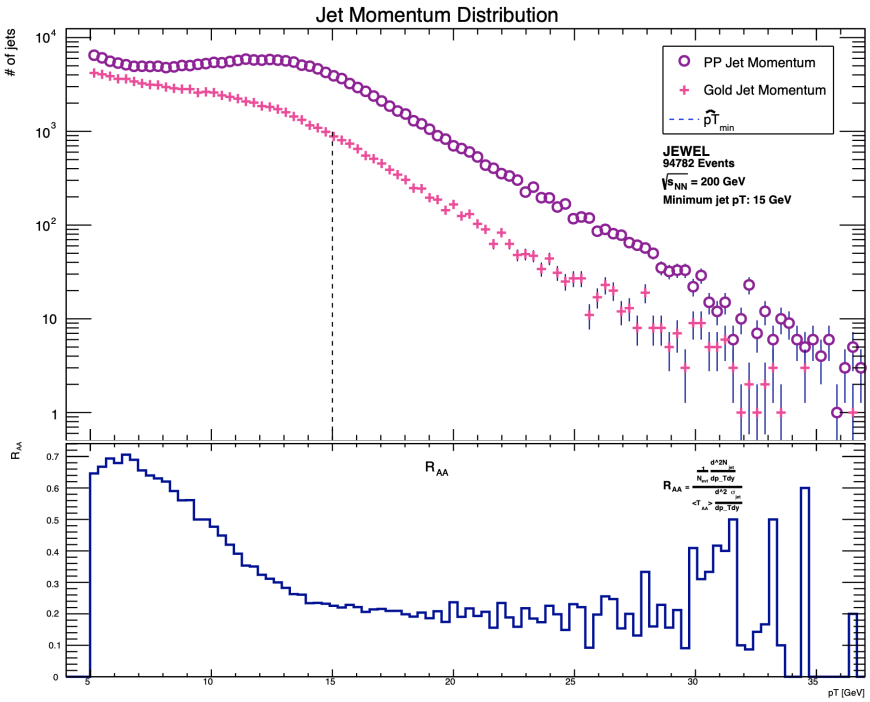

Figure 14: The top panel is a distribution of transverse momenta for each type of simulation. The bottom panel is the nuclear modification factor for each transverse momentum bin plotted. This shows jet quenching because the ratio above the bias limit (cutoff at the vertical dotted line) is less than 1, so there are fewer jets at those momenta in the gold-gold collisions than the proton-proton collisions.

lisions observed by detectors at RHIC, a more complete comparison between computational and experimental results is necessary.

5 Conclusion

This research demonstrates the promise of JEWEL for simulation of the collisions at RHIC, especially the kinds of collisions the sPHENIX detectors are observing. The minimum bias distribution and the nuclear modification factor both indicate that the simulation results are in line with analytical knowledge. The minimum bias distributions for quenched and unquenched simulations show that the jet momentums for simulations that interact with the QGP medium are, in general, lower energy than the jets from simulations that do not have any interaction with the QGP. This is further proven because the nuclear modification factor, or R_{AA} value, is less than 1 throughout the entire momentum region considered by this study.

Further investigation into the nuclear modification factor for the minimum bias distribution will help advance the understanding of JEWEL's effectiveness at RHIC's energy regimes. Additionally, fitting the modified Hagedorn function to the minimum bias distribution will offer further insight into the specific jet momentum distributions present in the JEWEL simulations.

There are also ways to increase the realistic nature of the simulation. In particular, only hard-scattering processes are being considered, and adding radiative energy loss (soft scattering) could influence the extent of quenching observed. JEWEL has existing infrastructure to include both scattering types. Only very central collisions are simulated here as well, with no less than 0.9 times the cross section overlapping during the collision. Considering less central collisions lowers the collision momentum even more, and would be a more complete way to determine the low energy applicability of JEWEL.

Currently, FastJet is only finding jets with one fixed radius. In order to make sure that every jet Jewel produces is considered, variation in jet radius and optimizing that radius for each event could help to make sure that the momentum distributions are accurate. Finally, the best way to check if the Jewel simulations are realistic is to compare to data taken on sPHENIX. Comparisons between the jet quenching done in the Jewel simulations with actual observed jet quenching can be performed as soon as the data from the experiment is available and reliable. The results of this research suggest that Jewel is an effective tool for simulating heavy ion collisions at RHIC. This research will continue to provide valuable insight into expectations and ideal results from this exciting experiment.

List of Figures

References

[1] Wikipedia contributors, *Standard model — Wikipedia, the free encyclopedia*, https://en.wikipedia.org/wiki/Standard_Model, [Online; accessed 19-March-2024], 2024.

[2] K. Zapp, J. Stachel, and U. A. Wiedemann, The European Physical Journal C, 10.1140/epjc/s10052-009-0941-2 (2009).

[3] C. Lorce, A. Metz, B. Pasquini, and S. Rodini, Deep Inelastic Scattering Workshop (2022).

[4] A. Kalweit, *The physics of heavy ion collisions*, Lecture Series, September 2017, CERN-Fermilab School, Geneva, Switzerland, 2017.

[5] W. Busza, K. Rajagopal, and W. van der Schee, Annual Review of Nuclear and Particle Science **68**, 339 (2018).

[6] K. M. Walsh, Brookhaven National Laboratory Newsroom, [Online; accessed 19-March-2024] (2017).

[7] H. Elfner and B. Müller, 10.48550/arXiv.2210.12056 (2022).

[8] A. Deur, S. Brodsky, and G. de Teramond, Progress in Particle and Nuclear Physics **90**, 10.1016/j.ppnp.2016.04.003 (2016).

[9] M. N. Chernodub, Modern Physics Letters A **29**, 1450162 (2014).

[10] *Evolution of the early universe*, https://phys.libretexts.org/@go/page/4956, [Online; accessed 19-March-2024], 2022.

[11] Q. Wang, P.-P. Yang, and F.-H. Liu, Results in Physics **12**, 259 (2019).

[12] A. Collaboration, "ATLAS feature: looking inside trillion degree matter", General Photo, 2022.

[13] L. Cunqueiro and A. M. Sickles, Progress in Particle and Nuclear Physics **124**, 103940 (2022).

[14] H. Jiang, *sPHENIX calorimeters*, [Online; accessed 01-April-2024], 2023.

[15] R. Belmont, J. Brewer, Q. Brodsky, P. Caucal, M. Connors, M. Djordjevic, R. Ehlers, M. A. Escobedo, E. G. Ferreiro, G. Giacalone, Y. Hatta, J. Holguin, W. Ke, Z.-B. Kang, A. Kumar, A. Mazeliauskas, Y. Mehtar-Tani, G. Nukazuka, D. Pablos, D. V. Perepelitsa, K. Rajagopal, A. M. Sickles, M. Strickland, K. Tywoniuk, I. Vitev, X.-N. Wang, Z. Yang, and F. Zhao, 10.1016/j.nuclphysa.2024.122821 (2023).

[16] Brookhaven National Laboratory, *RHIC Accelerators*, https://www.bnl.gov/rhic/complex.php, [Online; accessed 19-March-2024].

[17] M. Lamont, *The LHC's First Long Run*, [Online; accessed 19-March-2024], 2013.

[18] K. M. Walsh, Brookhaven National Laboratory Newsroom, [Online; accessed 19-March-2024] (2016).

[19] J. Kvapil, G. Borca-Tasciuc, H. Bossi, K. Chen, Y. Chen, Y. C. Morales, H. D. Costa, C. D. Silva, C. Dean, J. Durham, S. Fu, C. Hao, P. Harris, O. Hen, H. Jheng, Y. Lee, P. Li, X. Li, Y. Lin, M. X. Liu, A. Olvera, M. L. Purschke, M. Rigatti, G. Roland, J. Schambach, Z. Shi, N. Tran, N. Wuerfel, B. Xu, D. Yu, and H. Zhang, 10.48550/arXiv.2312.15104 (2023).

[20] T. Sjöstrand, L. Lönnblad, S. Mrenna, and P. Skands, *PYTHIA 6.3 physics and manual*, 2003.

[21] M. L. Miller, K. Reygers, S. J. Sanders, and P. Steinberg, Annual Review of Nuclear and Particle Science **57**, 205 (2007).

[22] M. R. Whalley, D. Bourilkov, and R. C. Group, (2005).

[23] R. K. Elayavalli and K. C. Zapp, Journal of High Energy Physics **2017**, 10.1007/jhep07(2017)141 (2017).

[24] G. P. Salam, The European Physical Journal C **67**, 637 (2010).

[25] M. Cacciari, G. P. Salam, and G. Soyez, The European Physical Journal C **72**, 10.1140/epjc/s10052-012-1896-2 (2012).

[26] s. Collaborators, "sEPD project summary".